CMS Physics Analysis Summary

Contact: cms-pag-conveners-susy@cern.ch 2016/10/20

Search for direct top squark pair production in the dilepton final state at $\sqrt{s} = 13$ TeV

The CMS Collaboration

Abstract

We present a search for direct top squark production in the opposite-sign dilepton channel using LHC pp collision data at $\sqrt{s} = 13$ TeV amounting to 12.9 fb^{-1} collected by the CMS detector in 2016. The search is performed in final states with two leptons, electrons or muons, jets, of which at least one is b-tagged, and missing transverse momentum. Signal regions are defined using transverse mass variables, which efficiently separate the signal from the dominant top-quark pair background. No significant deviation from the background prediction is observed. Exclusion limits are set in the context of a simplified supersymmetric model with pair production of top squarks that each decay to a top quark and a neutralino. For neutralino masses below 150 GeV, masses of the lightest top squark below 650 GeV are excluded at a confidence level of 95%.

1 Introduction

Supersymmetry (SUSY) [1–8] is a well-motivated theory beyond the standard model (SM) which provides solutions to several open questions in particle physics, e.g. the cancellation of quadratically divergent loop corrections to the squared mass of the Higgs boson. In *R*-Parity [9] conserving SUSY, the lightest SUSY particle (LSP) is stable and can be a viable dark matter candidate.

We present the result of a search for top squark pair production in a final state with two leptons, jets, and significant transverse momentum imbalance. Searches for this signature were previously published by the ATLAS [10] collaboration using 8 TeV proton-proton (pp) collision data and by CMS [11] on the 8 TeV data set. Results at 13 TeV were reported by the CMS collaboration [12, 13] and comprise the zero- and one-lepton channel. The search is performed using data from pp collisions, collected during 2016 at a center-of-mass energy of 13 TeV with the CMS detector at the LHC, corresponding to an integrated luminosity of 12.9 fb^{-1}. The results are interpreted in a simplified model describing the strong production of pairs of top squarks. The decay mode under consideration is shown in Fig. 1 and results are obtained as a function of the masses of the lightest top squark ($\tilde{\text{t}}$) and the lightest neutralino ($\tilde{\chi}_1^0$), denoted by $m_{\tilde{\text{t}}}$ and $m_{\tilde{\chi}_1^0}$, respectively.

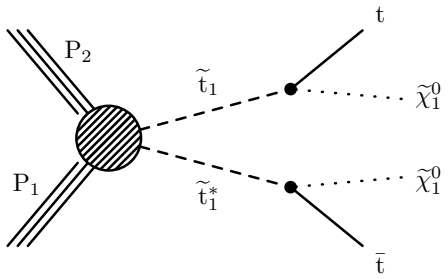

Figure 1: Production of a top squark pair ($\tilde{\text{t}}\tilde{\text{t}}^*$) in a simplified model of strongly produced top squark pairs. Each of the top squarks decays into a top quark and a neutralino ($\tilde{\chi}_1^0$).

When both top quarks decay leptonically, this process predicts a rather clean final state with two opposite-sign leptons, jets, and significant transverse momentum imbalance from the neutralinos and neutrinos. The search focuses on an efficient background reduction strategy using transverse mass variables [14] that suppress the large background of SM $\text{t}\bar{\text{t}}$ events by several orders of magnitude. The simulated predictions of the SM backgrounds are validated in data control samples that are orthogonal to the signal selection.

2 Event samples and object selection

2.1 Event samples

Collision data are selected by different triggers that require the presence of one or two leptons, electrons or muons. For the isolated dilepton triggers that accept the majority of events, the thresholds are no higher than 23 GeV (17 GeV) in the leading (sub-leading) lepton transverse momentum.

The $\text{t}\bar{\text{t}}$ and single top background samples are simulated using the POWHEG v2 [15, 16] event generator and are normalized to NNLO cross sections [17–23]. Drell-Yan and $\text{t}\bar{\text{t}}\text{Z}$ events are generated with MG5_AMC@NLO [24] at leading order (LO) and their cross sections are computed at NNLO [25] and NLO respectively. Other backgrounds, which include the multibo-

son, $t\bar{t}W$, $t\bar{t}H$, tZq, and $t\bar{t}\gamma$ processes, are generated using MG5_AMC@NLO program at next-to-leading order and are normalized to the most precise available cross section, corresponding to NLO accuracy in most cases. Generated events are interfaced to PYTHIA v8.2 [26, 27] using the CUETP8M1 tune [28, 29] to simulate parton showering, hadronization, and the underlying event. These events are processed with a GEANT4-based simulation model [30] of the CMS detector.

Signal samples are generated with MG5_AMC@NLO at LO precision interfaced with PYTHIA v8.2 for stop quark masses ranging from 150 GeV to 1.2 TeV and LSP masses from 1 GeV up to 650 GeV. The signal production cross sections are normalized at NLO+NLL level [31]. The detector simulation is performed using the CMS fast simulation package [32].

The simulated samples include additional simultaneous interactions per bunch crossing (pileup), with distributions that are weighted to match the observed data. Furthermore, simulated samples are weighted to reproduce the efficiency of the trigger selection, with typical values of $95\% - 99\%$ depending on the momenta and pseudorapidity of the two leptons.

2.2 Object selection

Offline event reconstruction uses the CMS particle-flow (PF) algorithm [33] for particle identification. Lepton candidates (electrons or muons) are required to satisfy $p_T > 25\,\text{GeV}$ $(20\,\text{GeV})$ for the leading (sub-leading) lepton and $|\eta| < 2.4$. Consistency of the track with the selected primary vertex is enforced by vetoing lepton candidates with a significance of the transverse track impact parameter above 4, where the impact parameter is the minimum three-dimensional distance between the lepton trajectory and the primary vertex. Its significance is defined as the ratio of the impact parameter to its uncertainty. The longitudinal displacement from the primary collision vertex must also be less than 0.1 cm.

Lepton candidates are required to be isolated. For each lepton candidate, a cone around the track direction at the event vertex is constructed. To enhance the acceptance of signal events that contain a large amount of hadronic energy, we use a p_T-dependent cone radius of $R = (0.2,\ 10\,\text{GeV}/p_T[\text{GeV}],\ 0.05)$ for $(p_T < 50\,\text{GeV},\ 50\,\text{GeV} < p_T < 200\,\text{GeV},\ p_T > 200\,\text{GeV})$, respectively. The scalar sum of the p_T of all particles reconstructed with the PF algorithm within the cone, consistent with arising from the chosen event production (primary) vertex, and corrected for pileup activity, is calculated excluding the lepton candidate. The relative mini-isolation discriminant, I_{mini}, is defined as the ratio of this sum to the p_T of the lepton candidate. Because the mini-isolation cone is typically too small to reject non-prompt low-p_T leptons originating from low-p_T b-quarks, we additionally require the lepton to pass a threshold for the p_T^{ratio} variable, defined as the ratio of the lepton p_T to the p_T of the jet matched to the lepton. If no jet is geometrically matched within $\Delta R < 0.4$, then this condition is automatically fulfilled. In order to recover leptons which accidentally overlap with jets in boosted topologies, leptons failing the p_T^{ratio} threshold are recovered when they pass a threshold for the p_T^{rel} variable, which is calculated by subtracting the lepton from the momentum vector of the geometrically matched jet and then finding the component of the lepton which is transverse to this new vector. In summary, the lepton isolation criterion is $I_{\text{mini}} < 0.09 \wedge (p_T^{\text{ratio}} > 0.84 \vee p_T^{\text{rel}} > 7.2)$.

Jets are clustered from PF candidates using the anti-k_t algorithm [34] with a distance parameter of $R = 0.4$. The influence of pileup is mitigated using the charged hadron subtraction (CHS) technique, by subtracting the energy of charged hadrons not coming from the primary vertex [35]. Jets are calibrated in simulation and in data separately, accounting for deposits from pileup and the imperfect detector response. Corrected jets are cleaned from anomalous energy deposits and instrumental noise if they pass $p_T > 30$ GeV and $|\eta| < 2.4$. To disambiguate jets

Table 1: Overview of the preselection.

leptons	2 (e or μ), opposite charge
$m(ll)$	≥ 20
$\lvert M_Z - m(ll)\rvert$	$> 15\,\text{GeV}$, same flavor only
N_{jets}	≥ 2
N_{bjets}	≥ 1
$E_{\text{T}}^{\text{miss}}$	> 80 GeV
S	$> 5\,\text{GeV}^{1/2}$
$\cos\Delta\phi(E_{\text{T}}^{\text{miss}}, j_1)$	< 0.80
$\cos\Delta\phi(E_{\text{T}}^{\text{miss}}, j_2)$	< 0.96

and leptons, jets that are found within a cone of $R = 0.4$ around any of the isolated leptons are removed from the set of selected jets.

The missing transverse energy $E_{\text{T}}^{\text{miss}}$ is defined as the magnitude of the negative vector sum of all particle flow candidates reconstructed in an event and is corrected for the effect of the jet energy corrections.

The multivariate b-tagging discriminator "Combined Secondary Vertex Tagger" (CSVv2) [36] is used to identify jets that originate from hadronization of b-quarks. The chosen "medium" working point has a mistag rate of approximately 1% for light flavor jets and a corresponding tagging efficiency of 55% to 65% depending on the jet transverse momentum and pseudorapidity.

3 Search strategy

We select events with a pair of leptons (electrons or muons) with opposite charge and require a minimum invariant mass of the lepton pair of 20 GeV in order to suppress backgrounds with misidentified leptons from the hadronization of jets. Events with additional leptons with $p_{\text{T}} > 15\,\text{GeV}$ and satisfying a looser isolation criterion of $I_{\text{mini}} < 0.4$ are vetoed. In case of a same-flavor lepton pair, we suppress contributions from SM Drell-Yan production with a veto on the dilepton mass, $|M_Z - m(ll)| > 15\,\text{GeV}$. To further suppress this and other vector boson backgrounds, we require at least two jets and at least one b-tagged jet. After requiring $E_{\text{T}}^{\text{miss}} > 80$ GeV, there remains a small background with vector bosons and high energetic jets that are severely mismeasured and hence pass the $E_{\text{T}}^{\text{miss}}$ requirement. We remove this background by defining $S = E_{\text{T}}^{\text{miss}}/\sqrt{H_T}$ and requiring $S > 5$ GeV$^{1/2}$ and, furthermore, by placing a requirement on the angular separation of $\vec{E}_{\text{T}}^{\text{miss}}$ and the two leading jets in the azimuthal plane. The selection above is summarized in Table 1 and defines an event sample which is dominated by events with top quark pairs which decay to a dilepton final state.

The main search variable in this analysis is

$$M_{T2}(\ell\ell) = \min_{\vec{p}_{\text{T1}}^{\text{miss}} + \vec{p}_{\text{T2}}^{\text{miss}} = \vec{E}_{\text{T}}^{\text{miss}}} \left(\max \left[M_T(\vec{p}_{\text{T}}^{\text{vis1}}, \vec{p}_{\text{T1}}^{\text{miss}}), M_T(\vec{p}_{\text{T}}^{\text{vis2}}, \vec{p}_{\text{T2}}^{\text{miss}}) \right] \right) \quad (1)$$

where the choice $\vec{p}_{\text{T}}^{\text{vis1,2}} = \vec{p}_{\text{T}}^{\ell 1,2}$ corresponds to the definition used in Ref. [37]. The calculation of $M_{T2}(\ell\ell)$ is performed through the algorithm discussed in Ref. [38]. When $\vec{E}_{\text{T}}^{\text{miss}}$ falls within the smaller of the two transverse plane opening angles defined by the leptons, it follows that $M_{T2}(\ell\ell) = 0$ because the minimization procedure will find a partitioning where $\vec{p}_{\text{T1,2}}^{\text{miss}}$ and $\vec{p}_{\text{T}}^{\text{l1,2}}$

are both parallel. It can furthermore be shown [14], that the construction of $M_{T2}(\ell\ell)$ via Eq. 1 has an endpoint at the parent particles mass, that is M_{W}, for both dileptonic $\mathrm{t\bar{t}}$ and WW events.

The key feature of this analysis is that the presence of additional invisible particles, e.g. the LSP, break the correlation between the $E_{\mathrm{T}}^{\mathrm{miss}}$ and the lepton transverse momenta that define the M_{W} endpoint. Hence, we expect the events predicted by the supersymmetric signal depicted in Fig. 1 to populate the tails of this distribution. The distribution of $M_{T2}(\ell\ell)$ after the preselection is shown in Fig. 2(a) including a signal with a benchmark mass configuration of $m_{\tilde{t}} = 650$ GeV and $m_{LSP} = 1$ GeV, as well as a more compressed signal scenario with $m_{\tilde{t}} = 500$ GeV and $m_{LSP} = 250$ GeV.

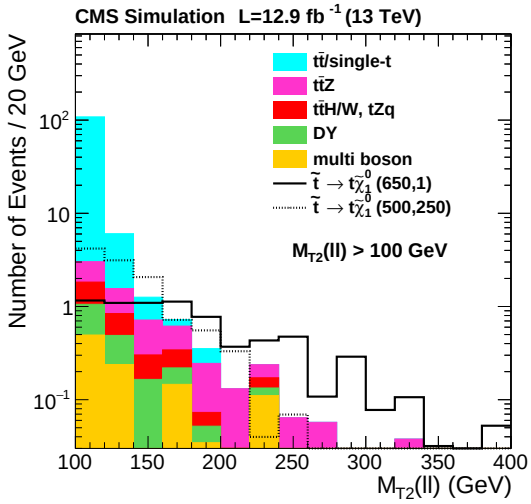

(a) $M_{T2}(\ell\ell)$

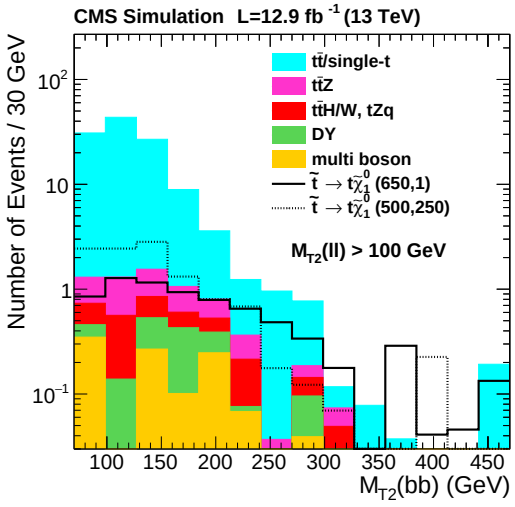

(b) $M_{T2}(bb)$

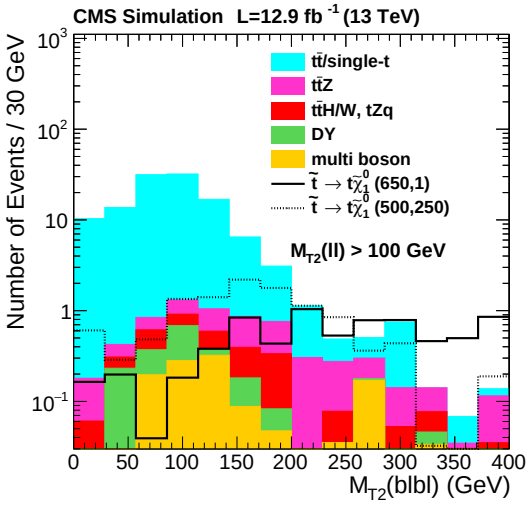

(c) $M_{T2}(b\ell b\ell)$

Figure 2: Distributions of $M_{T2}(\ell\ell)$, $M_{T2}(bb)$, and $M_{T2}(b\ell b\ell)$ after preselection and requiring $M_{T2}(\ell\ell) > 100$ GeV.

We refine the analysis by defining two more observables. For $M_{T2}(bb)$ we define $\vec{p}_{\mathrm{T}}^{\,\mathrm{vis1,2}} = \vec{p}_{\mathrm{T}}^{\,b1,2}$ and for $M_{T2}(b\ell b\ell)$ we define $\vec{p}_{\mathrm{T}}^{\,\mathrm{vis1,2}} = \vec{p}_{\mathrm{T}}^{\,b1,2} + \vec{p}_{\mathrm{T}}^{\,l1,2}$. For both observables, two b-tagged jets are required. If only one can be found in the event, the jet with the highest p_T that does not pass the b-tag selection is taken instead. The ambiguity when pairing leptons with b-jets for $M_{T2}(b\ell b\ell)$ is resolved by selecting the configuration which minimizes the maximum invariant mass of

the two lepton-jet pairs. After a tight threshold of $M_{T2}(\ell\ell) > 100$ GeV these variables still exhibit significant discrimination power. This is shown in Fig. 2(b) for $M_{T2}(bb)$ and Fig. 2(c) for $M_{T2}(b\ell b\ell)$, respectively.

Based on sensitivity studies on a wide range of supersymmetric mass configurations and the selection thresholds for the three search variables, $M_{T2}(\ell\ell)$, $M_{T2}(bb)$ and $M_{T2}(b\ell b\ell)$, the signal regions as listed in Table 2 are chosen. There is no overlap between any of the signal regions with other signal or control regions used in the following.

Table 2: Definition of the signal regions.

$M_{T2}(b\ell b\ell)$ (GeV)	$M_{T2}(bb)$ (GeV)	$100 \leq M_{T2}(\ell\ell) < 140$ GeV	$140 \leq M_{T2}(\ell\ell) < 240$ GeV	$M_{T2}(\ell\ell) \geq 240$ GeV
$0-100$	$70-170$	SR0	SR6	SR12
	≥ 170	SR1	SR7	
$100-200$	$70-170$	SR2	SR8	
	≥ 170	SR3	SR9	
≥ 200	$70-170$	SR4	SR10	
	≥ 170	SR5	SR11	

4 Background prediction

The remaining backgrounds from SM processes in the search regions after the event selection are single-t and $t\bar{t}$ events with either severely mismeasured E_T^{miss} or misidentified leptons, followed by top quark pair production in association with a Z, W, or a Higgs boson ($t\bar{t}Z$, $t\bar{t}W$, $t\bar{t}H$, tqZ), and Drell-Yan and multi-boson production (WWW, WWZ, WZZ, and ZZZ).

4.1 Top quark background

Both single-top and top-pair production populate low regions in the distributions of the three analysis variables $M_{T2}(\ell\ell)$, $M_{T2}(b\ell b\ell)$, and $M_{T2}(bb)$ if events are well measured. Studies based on simulation show two main sources for top quark background in the signal regions. First, a severe mismeasurement of jet energy caused by losses of photons and neutral hadrons showering in masked channels of the calorimetry can induce E_T^{miss} mismeasurement and promote an otherwise well-measured event to the signal regions. A control region $|m(ll) - m_Z| < 15$ GeV in the same-flavor channel can be used to constrain any mismodeling of this rare effect from comparing the E_T^{miss} tail between data and simulation. It is found that for the available data set, the simulation very well predicts such mismeasurements and that no sign of unaccounted effects in the E_T^{miss} measurement is observed. Furthermore, the modeling of the tail of the analysis variables is validated in control regions with a veto on b-tagged jets and inverted requirements on N_{jets} and/or E_T^{miss} and S. As an example, Fig. 3a shows the $M_{T2}(\ell\ell)$ distribution in the opposite flavor channel with $N_{bjets} \geq 1$, $N_{jets} \geq 2$, $E_T^{miss} < 80$, and no requirement on S. No significant sign of mismodeling is found in any of the control regions over at least three orders of magnitude. The uncertainties from experimental effects as described in Sec. 5 are shown with a hatched band.

Second, an electron or muon may fail the identification requirements or the event may have a tau lepton produced in a W decay. If there is a misidentified lepton from the hadronization of a b-quark or a charged hadron misidentified as a prompt lepton in the same event, the reconstructed value for $M_{T2}(\ell\ell)$ need not respect the W mass endpoint. For this contribution, we select events with one additional lepton selected by loose isolation requirements (2 tight leptons, one loosely isolated lepton) on top of the selection in Table 1. In order to mimic the lost prompt lepton background, we recompute $M_{T2}(\ell\ell)$ by combining each of the isolated leptons

with the extra lepton in both data and simulation. Since the transverse momentum balance is not significantly changed by lepton misidentification, the $E_{\mathrm{T}}^{\mathrm{miss}}$ observable is not modified. The resulting $M_{T2}(\ell\ell)$ distribution is shown in Fig. 3b. We observe an overall good agreement between simulation and data, indicating that simulation describes such backgrounds well.

Based on the statistical precision of these control regions, we assign a conservative uncertainty between 50% for the lowest regions in $M_{T2}(\ell\ell)$ up to 100% in the highest region where $M_{T2}(\ell\ell) > 240\,\mathrm{GeV}$ and proceed to predict the background from single-top and $\mathrm{t\bar{t}}$ production by normalizing simulated templates in data events in the selection defined by $M_{T2}(\ell\ell) < 100$ GeV. In this way, experimental uncertainties affecting the overall normalization are largely reduced.

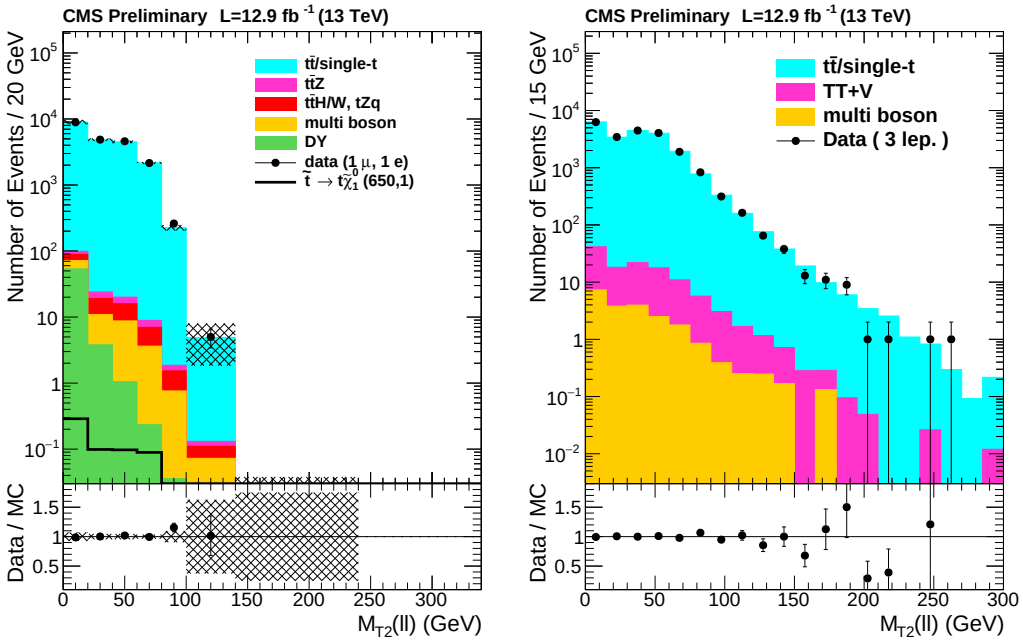

(a) $e\mu$ control region with $N_{\mathrm{jets}} \geq 2$, $N_{\mathrm{bjets}} \geq 1$ and $E_{\mathrm{T}}^{\mathrm{miss}} < 80$ GeV

(b) 2 tight, 1 loose

Figure 3: $M_{T2}(\ell\ell)$ distributions in two control regions enriched by $t\bar{t}$ events. Simulated yields are normalized to data using the yields at $M_{T2}(\ell\ell) < 100$ GeV.

4.2 tt+X background

Top quark and top quark pair production in association with a boson ($\mathrm{t\bar{t}Z}$, $\mathrm{t\bar{t}W}$, $\mathrm{t\bar{t}H}$, $tq\mathrm{Z}$) form an irreducible background in decay channels where the bosons decay to leptons or neutrinos. Among these, the $\mathrm{t\bar{t}Z}$ background with a Z boson decay via $Z \to \nu\bar{\nu}$ providing extra genuine $E_{\mathrm{T}}^{\mathrm{miss}}$, is the dominant one. The overall normalization of this contribution is measured in the decay mode

$$\mathrm{pp} \to \mathrm{t\bar{t}Z} \to (t \to \mathrm{b}\ell^{\pm}\nu)(\mathrm{t} \to \mathrm{bjj})(\mathrm{Z} \to \ell^{\pm}\ell^{\mp}),$$

in control regions with exactly three leptons ($\mu\mu\mu$, $\mu\mu e$, μee and eee) where the leading, subleading and trailing lepton transverse momentum are required to satisfy thresholds of 30, 20 and 10 GeV, respectively. The invariant mass of the two same-flavor leptons with opposite charge is required to satisfy $|\mathrm{m}_{\ell\ell} - \mathrm{M}_{\mathrm{Z}}| < 10$ GeV and is shown in Fig. 4a. The distribution of N_{bjets} is shown in Fig. 4b. In order to reach high $\mathrm{t\bar{t}Z}$ purity $N_{\mathrm{jets}} \geq 3$ and $N_{\mathrm{bjets}} \geq 1$ are required.

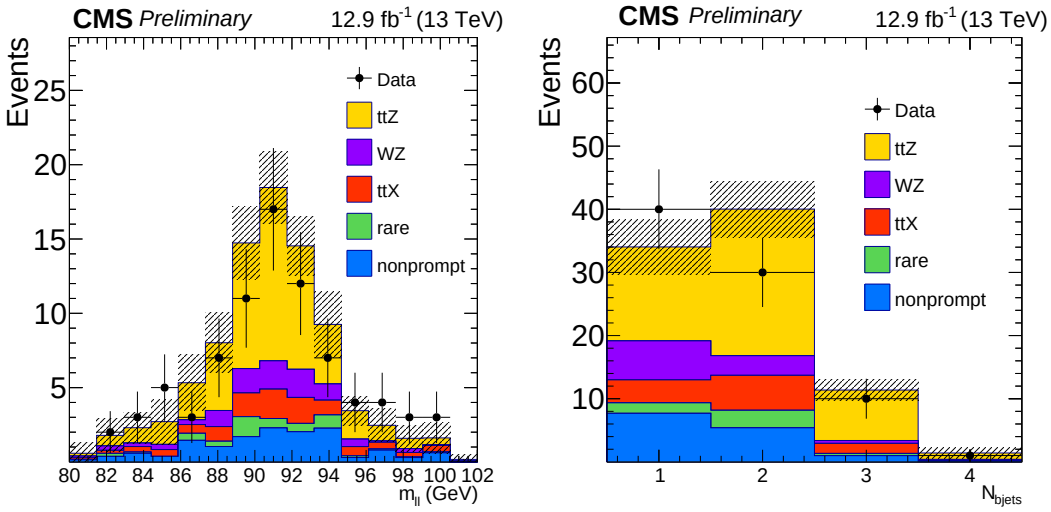

(a) Di-lepton invariant mass

(b) Number of b-tagged jets

Figure 4: Control region used for normalization of the $t\bar{t}Z$ process. The hatched band contains the uncertainties due to luminosity, jet energy scale, jet energy resolution, trigger efficiencies, b-tagging efficiencies, lepton selection efficiencies, pileup reweighting, scale and PDF uncertainties as well as the uncertainties due to non-prompt leptons and other SM processes.

The measurement of the signal strength

$$r = 0.89^{+0.18}_{-0.16}(\text{stat})\ ^{+0.13}_{-0.15}(\text{sys}) \tag{2}$$

combines all flavor channels and has been documented separately [39]. It is then used to normalize the $t\bar{t}Z$ background in the signal regions where the uncertainties on r are fully taken into account in the background prediction.

Furthermore, we constrain a potential mismodeling of the $t\bar{t}Z$ ($Z \to \nu\bar{\nu}$) distributions in a $t\bar{t}\gamma$ control sample by using the photon as proxy for the Z boson and adding its momentum to the $E_{\mathrm{T}}^{\mathrm{miss}}$. After suitable reweighting of the simulated boson momentum, which mitigates the difference between the massive Z boson and the massless photon, we find very good agreement between simulated $t\bar{t}\gamma$ and $t\bar{t}Z$ distributions. Repeating the exercise on data, we constrain the mismodeling to 20% and assign this as an additional uncertainty.

4.3 Drell Yan and diboson background

Drell-Yan events provide no source for genuine $E_{\mathrm{T}}^{\mathrm{miss}}$ and therefore constitute only a small background component after the analysis selection. In order to measure the residual contribution, we select same-flavor di-lepton ($e^{\pm}e^{\mp}$, $\mu^{\pm}\mu^{\mp}$) events where we invert the Z-veto, b-jet requirements, and the angular separation requirements on jets and $E_{\mathrm{T}}^{\mathrm{miss}}$. We furthermore require $M_{T2}(\ell\ell) > 100$ GeV in order to select events with similar kinematical properties as in the search regions. The $M_{T2}(\ell\ell)$ distribution with this selection is presented in Fig. 5. From simulation, this selection is expected to contain about 85% Drell-Yan events. We calculate a scale factor of 1.30 ± 0.12 that we use to scale the simulated contribution. Applying the nominal requirements on $\Delta\phi(j_{1,2}, E_{\mathrm{T}}^{\mathrm{miss}})$, in turn, provides a control region with 70% diboson events based on simulation. It is shown in Fig. 5b and the corresponding scale factor is calculated to be 1.45 ± 0.26.

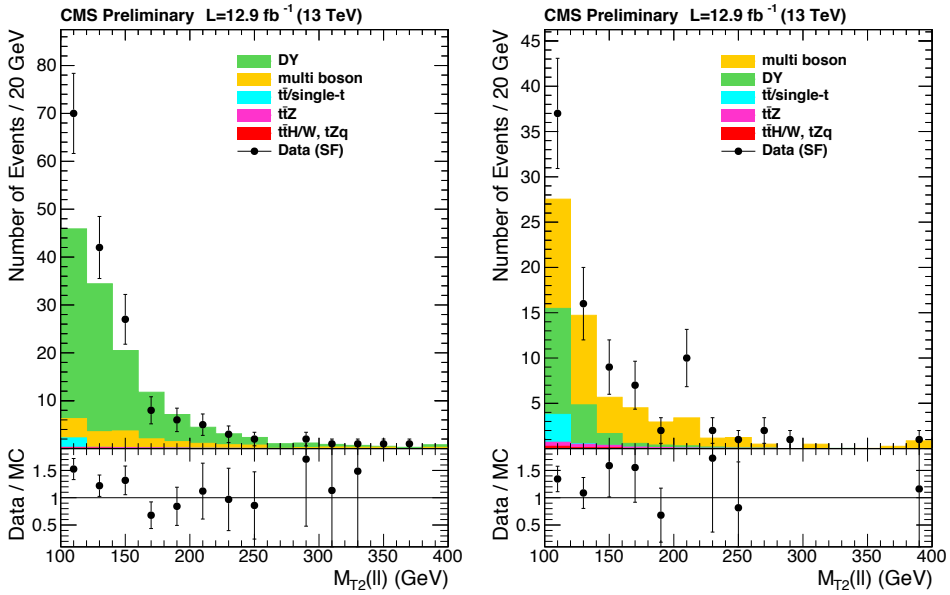

(a) (b)

Figure 5: Distributions of $M_{T2}(\ell\ell)$ in a DY (left) and diboson (right) dominated region for same-flavor ($ee/\mu\mu$) events falling within the Z-mass window, $N_{\text{jets}} \geq 2$ and no b-tagged jets.

5 Systematic uncertainties and signal acceptance

The uncertainty on the integrated luminosity is 6.2%. Simulated samples are reweighted according to the distribution of the true number of interactions at each bunch crossing. The uncertainty on the total inelastic pp cross section, which affects the pileup estimate, is 5% and leads to uncertainties of approx. 1–3% on the expected yields.

Reconstructed lepton selection efficiencies are measured with a tag-and-probe method using $Z \to ll$ events in bins of p_{T} and pseudorapidity of leptons and the total hadronic activity in the vicinity of the lepton. These measurements are performed separately in data and in simulation. Typical values range from 70% to 80% and scale factors are applied to correct the differences between data and simulation. Their uncertainties are less then 3% per lepton in most search and control regions.

Uncertainties on the jet energy calibration are estimated by shifting the energy of jets in the simulation up and down by one standard deviation. Depending on transverse momentum and pseudorapidity, the uncertainty on the jet energy scale is typically 1–5% on the simulated yields, except in the lowest regions in $M_{T2}(\ell\ell)$ where it can increase to up to 30%. In addition, the energy scale of deposits from soft particles that are not clustered in jets are varied within uncertainties and amount to up to 3.5% with a similar increase up to 25% in the lowest $M_{T2}(\ell\ell)$ region. The observed differences between the varied and the original results are taken as uncertainty for the background components which are taken from simulation. The b-tagging efficiency in the simulation is corrected using scale factors determined from the data [40] and uncertainties are propagated to all simulated events. These contribute an uncertainty of about 1–5% on the predicted yields depending on transverse momentum and pseudorapidity of the jet. Efficiencies of the dilepton triggers are measured in data that are selected independently by the presence of jets and by $E_{\text{T}}^{\text{miss}}$ requirements. Typical values range from 95% to 99% with uncertainties close to 1%, depending on the momenta and pseudorapidity of the leptons.

Table 3: Minimal and maximal relative errors for the systematic uncertainties over all signal regions in Fig. 9. Numbers are given relative to the total background contribution per signal region.

systematic	impact on total prediction (%)
MC statistics	4 - 40
pile-up	< 3
JEC	< 30
unclustered energy	< 25
top-p_{T}	< 3
trigger efficiency	< 1
lepton efficiency	< 3
b-tagging efficiency (heavy flavor)	< 4
b-tagging efficiency (light flavor)	< 5
top background	< 50
$t\bar{t}Z$ background	< 12
multiboson background	< 10
$t\bar{t}X$ (excl. $t\bar{t}Z$) background	< 8
DY background	< 12

Motivated by measurements at $\sqrt{s} = 8\,\mathrm{TeV}$, simulated $\mathrm{t\bar{t}}$ events are weighted within uncertainties of the modeling of the top quark transverse momentum [41], while preserving the overall normalization. The difference relative to the unweighted $\mathrm{t\bar{t}}$ sample is assigned as a systematic uncertainty which typically contributes about 1–3% on the predicted yields.

Uncertainties on the scale factors for single top and top-quark pair production, Drell-Yan and diboson backgrounds are taken into account as described in Sec. 4. For the small contribution from top-quark pair production in association with a W or a Higgs boson, we assess an uncertainty of 20% on the cross section. Rare SM processes like multibosons are assigned a 50% systematic uncertainty. In addition, all of the experimental uncertainties described above are evaluated for each of these processes in all signal regions. The statistical uncertainties due to the limited amount of simulated events and the Poissonian uncertainties from normalization region measurements are treated fully uncorrelated and amount to up to 40%. A summary of the systematic uncertainties on the background prediction is presented in Table 3.

Most of the sources of systematic uncertainties affect the prediction of both the signal and the background estimates. They are evaluated separately for the backgrounds and each SUSY particle mass configuration. We estimate the effect of missing higher-order corrections on the signal acceptance by varying the renormalization and factorization scale [42, 43] up and down by a factor of 2 and find uncertainties of typically $< 1\%$. The same variations have a negligible effect on the simulated background. The modeling of initial-state-radiation (ISR) is relevant for the signal modeling in cases where the stop and the LSP mass are similar. The uncertainty is determined by comparing the simulated and observed spectra of the number of ISR jets in $\mathrm{t\bar{t}}$ events. The effect is generally found to be small, although in scenarios with a compressed mass spectrum the effect can be as large as 30%. An uncertainty on potential differences of the modeling of $E_{\mathrm{T}}^{\mathrm{miss}}$ in data and the fast simulation of the CMS detector is evaluated by comparing the reconstructed $E_{\mathrm{T}}^{\mathrm{miss}}$ with the $E_{\mathrm{T}}^{\mathrm{miss}}$ obtained using generator-truth information. This uncertainty ranges up to 20%. Uncertainties due to luminosity, ISR recoil, $E_{\mathrm{T}}^{\mathrm{miss}}$ resolution, b-tagging and lepton efficiencies are treated as correlated across search regions. No additional uncertainty from variations of the PDF set is taken as it is found to be mostly redundant with the recoil ISR uncertainty.

6 Results

Using 12.9 fb^{-1} data, we observe no significant excess beyond the SM prediction. Results split for each signal region are shown in Figs. 6 and 7 and in Table 4.

For setting limits, a likelihood function is formed from all search regions containing Poisson probability functions for all data regions. Same-flavor and opposite-flavor signal regions are kept separate as shown in Table 4. The correlations of uncertainties in Sec. 5 are fully taken into account. A profile likelihood ratio in the asymptotic approximation [44] is used as the test statistic. Limits are then calculated at the 95% confidence level (CL) using the asymptotic CLs criterion [45, 46]. We interpret the result in the mass plane of $\tilde{t}$ and $\tilde{\chi}_1^0$, assuming the top squarks to be unpolarized and show the result in Fig. 10.

Table 4: Yields for data and total expected background in each of the signal regions for same-flavor ($ee/\mu\mu$), different-flavor ($e\mu$) and all channels combined with all systematic uncertainties as described in Sec. 5.

	same-flavor		different-flavor		all	
signal region	expected	observed	expected	observed	expected	observed
0	29 ± 14	27	28 ± 14	40	56 ± 27	67
1	2.0 ± 1.1	3	1.0 ± 0.6	3	3.0 ± 1.5	6
2	15 ± 7	17	13 ± 7	18	28 ± 13	35
3	2.0 ± 0.9	2	1.1 ± 0.5	1	3.1 ± 1.3	3
4	0.09 ± 0.06	0	0.060 ± 0.035	0	0.15 ± 0.07	0
5	0.60 ± 0.27	1	0.9 ± 0.6	0	1.5 ± 0.8	1
6	0.26 ± 0.08	0	0.12 ± 0.09	0	0.37 ± 0.13	0
7	0.12 ± 0.06	0	0.013 ± 0.013	0	0.14 ± 0.05	0
8	0.53 ± 0.16	2	0.48 ± 0.18	0	1.00 ± 0.26	2
9	0.47 ± 0.22	0	0.050 ± 0.029	0	0.52 ± 0.22	0
10	0.23 ± 0.17	1	0.18 ± 0.07	1	0.41 ± 0.19	2
11	0.73 ± 0.32	0	0.24 ± 0.09	0	0.97 ± 0.34	0
12	0.18 ± 0.06	0	0.050 ± 0.016	0	0.22 ± 0.06	0

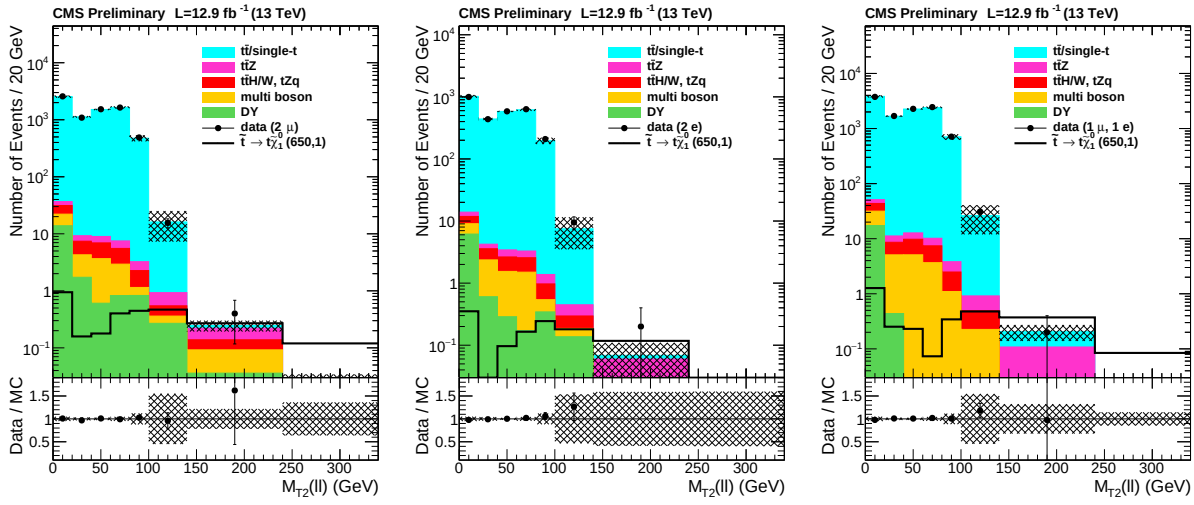

(a) $\mu\mu$ channel (b) ee channel (c) $e\mu$ channel

Figure 6: $M_{T2}(\ell\ell)$ distributions of observed events in $\mu\mu$, ee, $e\mu$ channels compared to the predicted SM backgrounds using simulation in the selection defined in Table 1. The shaded band covers all uncertainties discussed in the text.

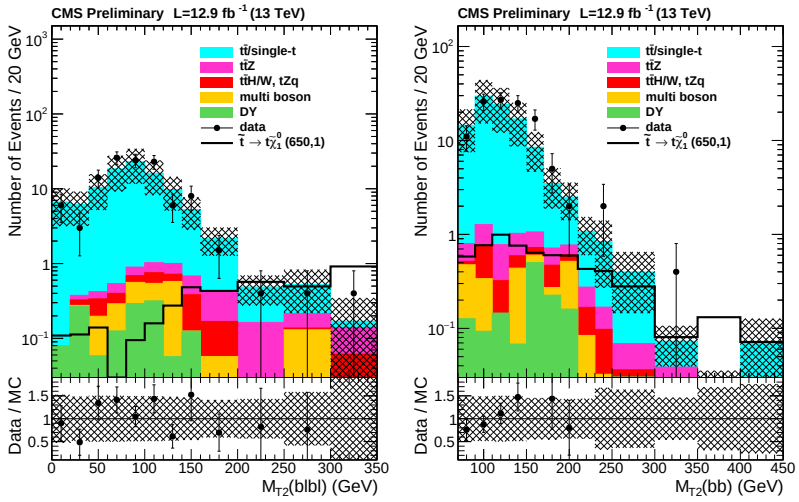

(a) all channels (b) all channels

Figure 7: Distributions of $M_{T2}(b\ell b\ell)$ and $M_{T2}(bb)$ in all flavor channels for the selection defined in Table 1 and for $M_{T2}(\ell\ell) > 100$ GeV. The shaded band covers all uncertainties discussed in the text.

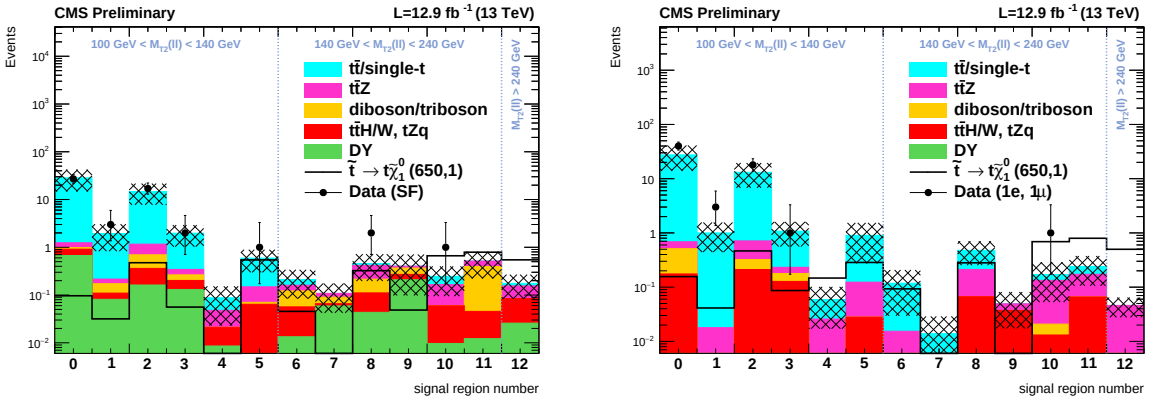

(a) $\mu\mu$ and ee channel (b) $e\mu$ channel

Figure 8: Predicted backgrounds and observed yields in each search region. The shaded band covers all uncertainties discussed in the text.

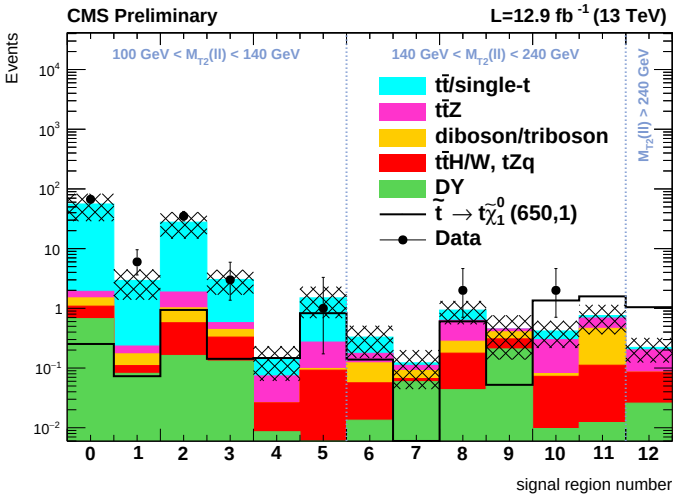

(a) All channels combined

Figure 9: Same as Fig. 8 but channels combined.

7 Conclusions

We presented a search for supersymmetry in a final state of two leptons, b jets, and large missing transverse momentum, originating from decays of pair-produced top squarks to two top quarks and neutralinos, with a subsequent fully leptonic decay of the top quarks. We used a data set corresponding to an integrated luminosity of 12.9 fb^{-1} of pp collisions collected in 2016 at a center-of-mass energy of 13 TeV with the CMS detector at the LHC. An efficient background reduction using dedicated kinematical variables was achieved, with in particular the large background of SM dilepton $\mathrm{t\bar{t}}$ events suppressed by several orders of magnitude.

We observe no evidence for an excess above the expected background from standard model processes. For neutralino masses of $m_{\tilde{\chi}_1^0} \leq 150$ GeV, mass configurations with $m_{\tilde{\mathrm{t}}} \leq 650$ GeV are excluded at a confidence level of 95%.

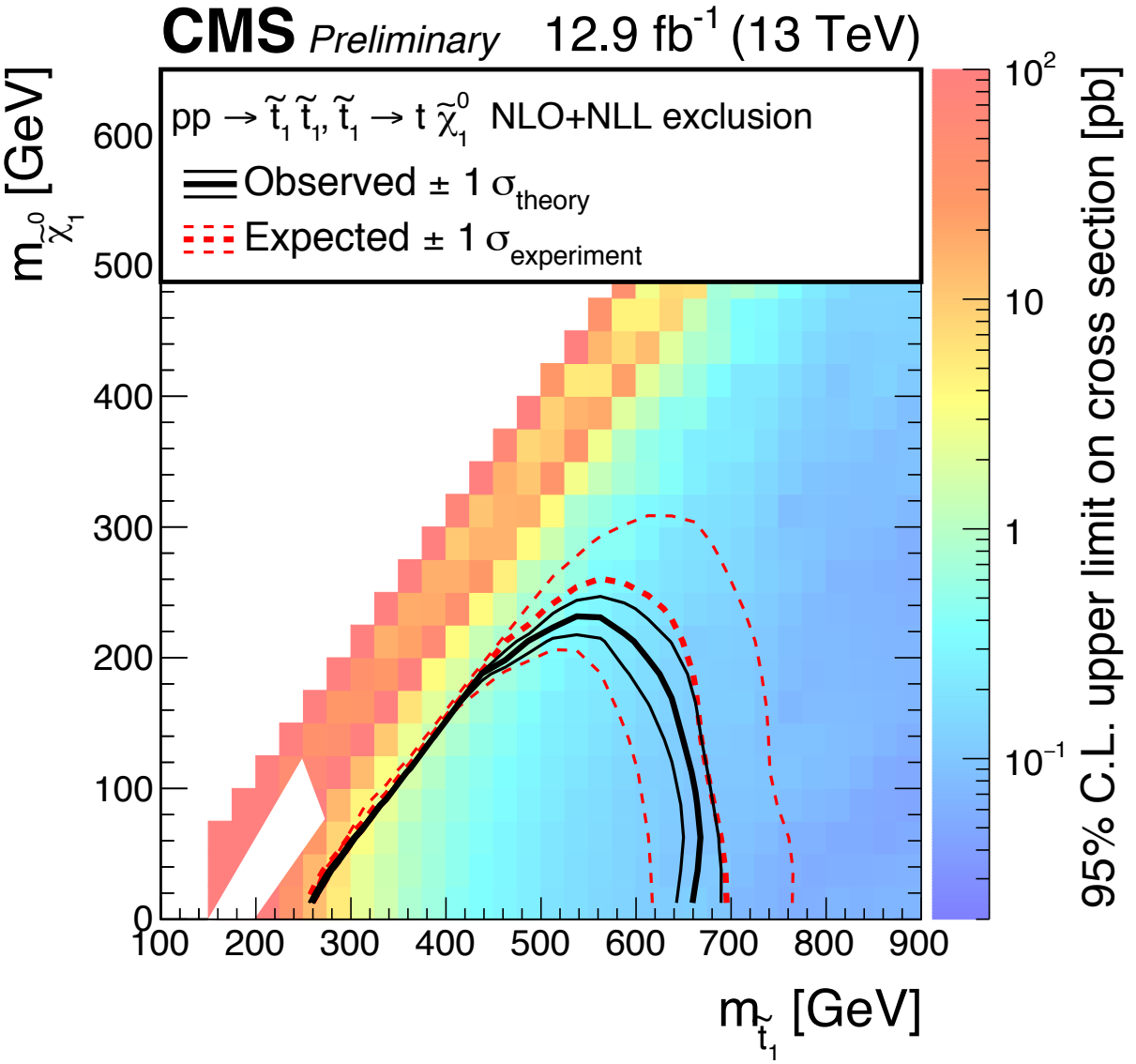

Figure 10: 95% CL expected and observed limits for the $\tilde{t} \to t\tilde{\chi}_1^0$ decay mode in the $m_{\tilde{t}}$, $m_{\tilde{\chi}_1^0}$ mass plane

References

[1] P. Ramond, "Dual theory for free fermions", *Phys. Rev. D* **3** (1971) 2415, doi:10.1103/PhysRevD.3.2415.

[2] Y. A. Golfand and E. P. Likhtman, "Extension of the algebra of Poincaré group generators and violation of P invariance", *JETP Lett.* **13** (1971) 323.

[3] A. Neveu and J. H. Schwarz, "Factorizable dual model of pions", *Nucl. Phys. B* **31** (1971) 86, doi:10.1016/0550-3213(71)90448-2.

[4] D. V. Volkov and V. P. Akulov, "Possible universal neutrino interaction", *JETP Lett.* **16** (1972) 438.

[5] J. Wess and B. Zumino, "A Lagrangian model invariant under supergauge transformations", *Phys. Lett. B* **49** (1974) 52, doi:10.1016/0370-2693(74)90578-4.

[6] J. Wess and B. Zumino, "Supergauge transformations in four dimensions", *Nucl. Phys. B* **70** (1974) 39, doi:10.1016/0550-3213(74)90355-1.

[7] P. Fayet, "Supergauge invariant extension of the Higgs mechanism and a model for the electron and its neutrino", *Nucl. Phys. B* **90** (1975) 104, doi:10.1016/0550-3213(75)90636-7.

[8] H. P. Nilles, "Supersymmetry, supergravity and particle physics", *Phys. Rep.* **110** (1984) 1, doi:10.1016/0370-1573(84)90008-5.

[9] G. R. Farrar and P. Fayet, "Phenomenology of the production, decay, and detection of new hadronic states associated with supersymmetry", *Phys. Lett. B* **76** (1978), no. 5, 575 – 579, doi:http://dx.doi.org/10.1016/0370-2693(78)90858-4.

[10] ATLAS Collaboration, "ATLAS Run 1 searches for direct pair production of third-generation squarks at the Large Hadron Collider", *Eur. Phys. J.* **C75** (2015), no. 10, 510, doi:10.1140/epjc/s10052-015-3726-9, 10.1140/epjc/s10052-016-3935-x, arXiv:1506.08616. [Erratum: Eur. Phys. J.C76,no.3,153(2016)].

[11] CMS Collaboration, "Search for supersymmetry in events with soft leptons, low jet multiplicity, and missing transverse energy in proton-proton collisions at $\sqrt{s}$=8 TeV", *Phys. Lett. B* **759** (2016) 9–35, doi:10.1016/j.physletb.2016.05.033, arXiv:1512.08002.

[12] CMS Collaboration, "Search for direct top squark pair production in the fully hadronic final state in proton-proton collisions at *sqrt*(s) = 13 TeV corresponding to an integrated luminosity of 12.9/fb", CMS Physics Analysis Summary CMS-PAS-SUS-16-029, 2016.

[13] CMS Collaboration, "Search for direct top squark pair production in the single lepton final state at $\sqrt{s} = 13$ TeV", CMS Physics Analysis Summary CMS-PAS-SUS-16-028, 2016.

[14] C. G. Lester and D. J. Summers, "Measuring masses of semiinvisibly decaying particles pair produced at hadron colliders", *Phys. Lett. B* **463** (1999) 99–103, doi:10.1016/S0370-2693(99)00945-4, arXiv:hep-ph/9906349.

[15] S. Alioli et al., "NLO single-top production matched with shower in POWHEG: s- and t-channel contributions", *JHEP* **09** (2009) 111, doi:10.1088/1126-6708/2009/09/111, arXiv:0907.4076.

[16] S. Alioli et al., "A general framework for implementing NLO calculations in shower Monte Carlo programs: the POWHEG BOX", *JHEP* **06** (2010) 043, doi:10.1007/JHEP06(2010)043, arXiv:1002.2581.

[17] M. Czakon and A. Mitov, "Top++: A Program for the Calculation of the Top-Pair Cross-Section at Hadron Colliders", *Comput. Phys. Commun.* **185** (2014) 2930, doi:10.1016/j.cpc.2014.06.021, arXiv:1112.5675.

[18] M. Aliev et al., "HATHOR: HAdronic Top and Heavy quarks crOss section calculatoR", *Comput. Phys. Commun.* **182** (2011) 1034–1046, doi:10.1016/j.cpc.2010.12.040, arXiv:1007.1327.

[19] M. Beneke, P. Falgari, S. Klein, and C. Schwinn, "Hadronic top-quark pair production with NNLL threshold resummation", *Nucl. Phys. B* **855** (2012) 695–741, doi:10.1016/j.nuclphysb.2011.10.021, arXiv:1109.1536.

[20] M. Czakon and A. Mitov, "NNLO corrections to top-pair production at hadron colliders: the all-fermionic scattering channels", *JHEP* **12** (2012) 054, doi:10.1007/JHEP12(2012)054, arXiv:1207.0236.

[21] M. Czakon and A. Mitov, "NNLO corrections to top pair production at hadron colliders: the quark-gluon reaction", *JHEP* **01** (2013) 080, doi:10.1007/JHEP01(2013)080, arXiv:1210.6832.

[22] M. Czakon, P. Fiedler, and A. Mitov, "Total Top-Quark Pair-Production Cross Section at Hadron Colliders Through $O(\frac{4}{S})$", *Phys. Rev. Lett.* **110** (2013) 252004, doi:10.1103/PhysRevLett.110.252004, arXiv:1303.6254.

[23] P. Kant et al., "HatHor for single top-quark production: Updated predictions and uncertainty estimates for single top-quark production in hadronic collisions", *Comput. Phys. Commun.* **191** (2015) 74–89, doi:10.1016/j.cpc.2015.02.001, arXiv:1406.4403.

[24] J. Alwall et al., "The automated computation of tree-level and next-to-leading order differential cross sections, and their matching to parton shower simulations", *JHEP* **07** (2014) 079, doi:10.1007/JHEP07(2014)079, arXiv:1405.0301.

[25] R. Gavin, Y. Li, F. Petriello, and S. Quackenbush, "FEWZ 2.0: A code for hadronic Z production at next-to-next-to-leading order", *Comput. Phys. Commun.* **182** (2011) 2388–2403, doi:10.1016/j.cpc.2011.06.008, arXiv:1011.3540.

[26] T. Sjöstrand, S. Mrenna, and P. Skands, "PYTHIA 6.4 physics and manual", *JHEP* **05** (2006) 026, doi:10.1088/1126-6708/2006/05/026, arXiv:hep-ph/0603175.

[27] T. Sjostrand et al., "An Introduction to PYTHIA 8.2", *Comput. Phys. Commun.* **191** (2015) 159–177, doi:10.1016/j.cpc.2015.01.024, arXiv:1410.3012.

[28] P. Skands, S. Carrazza, and J. Rojo, "Tuning PYTHIA 8.1: the Monash 2013 tune", *Eur. Phys. J. C* **74** (2014) 3024, doi:10.1140/epjc/s10052-014-3024-y, arXiv:1404.5630.

[29] CMS Collaboration, "Event generator tunes obtained from underlying event and multiparton scattering measurements", *Eur. Phys. J. C* **76** (2016) 155, doi:10.1140/epjc/s10052-016-3988-x, arXiv:1512.00815.

[30] GEANT4 Collaboration, "GEANT4 – a simulation toolkit", *Nucl. Instrum. Meth. A* **506** (2003) 250, doi:10.1016/S0168-9002(03)01368-8.

[31] C. Borschensky et al., "Squark and gluino production cross sections in pp collisions at $\sqrt{s}$ = 13, 14, 33 and 100 TeV", *Eur. Phys. J. C* **74** (2014), no. 12, 3174, doi:10.1140/epjc/s10052-014-3174-y, arXiv:1407.5066.

[32] S. Abdullin et al., "The fast simulation of the CMS detector at LHC", *J. Phys. Conf. Ser.* **331** (2011) 032049, doi:10.1088/1742-6596/331/3/032049.

[33] CMS Collaboration, "Commissioning of the Particle-Flow Reconstruction in Minimum-Bias and Jet Events from pp Collisions at 7 TeV", CMS Physics Analysis Summary CMS-PAS-PFT-10-002, CERN, 2010.

[34] M. Cacciari, G. P. Salam, and G. Soyez, "The anti-k_t jet clustering algorithm", *JHEP* **04** (2008) 063, doi:10.1088/1126-6708/2008/04/063, arXiv:0802.1189.

[35] CMS Collaboration, "Pileup Removal Algorithms", CMS Physics Analysis Summary CMS-PAS-JME-14-001, CERN, 2014.

[36] CMS Collaboration, "Identification of b-quark jets with the CMS experiment", *JINST* **8** (2013) 04013, doi:10.1088/1748-0221/8/04/P04013, arXiv:1211.4462.

[37] CMS Collaboration, "Search for direct pair production of scalar top quarks in the single- and dilepton channels in proton-proton collisions at $\sqrt{s} = 8$ TeV", *JHEP* **07** (2016) 027, doi:10.1007/JHEP07(2016)027, 10.1007/JHEP09(2016)056, arXiv:1602.03169. [Erratum: JHEP09,056(2016)].

[38] H.-C. Cheng and Z. Han, "Minimal Kinematic Constraints and m(T2)", *JHEP* **12** (2008) 063, doi:10.1088/1126-6708/2008/12/063, arXiv:0810.5178.

[39] CMS Collaboration, "Measurement of the top pair-production in association with a W or Z boson in pp collisions at 13 TeV", CMS Physics Analysis Summary CMS-PAS-TOP-16-017, CERN, 2016.

[40] CMS Collaboration, "Identification of b-quark jets with the CMS experiment", *JINST* **8** (2013) P04013, doi:10.1088/1748-0221/8/04/P04013, arXiv:1211.4462.

[41] CMS Collaboration, "Measurement of the differential cross section for top quark pair production in pp collisions at $\sqrt{s} = 8$ TeV", *Eur. Phys. J. C* **75** (2015), no. 11, 542, doi:10.1140/epjc/s10052-015-3709-x, arXiv:1505.04480.

[42] S. Catani, D. de Florian, M. Grazzini, and P. Nason, "Soft gluon resummation for Higgs boson production at hadron colliders", *JHEP* **07** (2003) 028, doi:10.1088/1126-6708/2003/07/028, arXiv:hep-ph/0306211.

[43] M. Cacciari et al., "The $t\bar{t}$ cross-section at 1.8 TeV and 1.96 TeV: a study of the systematics due to parton densities and scale dependence", *JHEP* **04** (2004) 068, doi:10.1088/1126-6708/2004/04/068, arXiv:hep-ph/0303085.

[44] G. Cowan, K. Cranmer, E. Gross, and O. Vitells, "Asymptotic formulae for likelihood-based tests of new physics", *Eur. Phys. J. C* **71** (2011) 1554, doi:10.1140/epjc/s10052-011-1554-0, 10.1140/epjc/s10052-013-2501-z, arXiv:1007.1727. [Erratum: Eur. Phys. J.C73,2501(2013)].

[45] T. Junk, "Confidence level computation for combining searches with small statistics", *Nucl. Instr. and Meth. A* **434** (1999) 435, doi:10.1016/S0168-9002(99)00498-2, arXiv:hep-ex/9902006.

[46] A. L. Read, "Presentation of search results: the CL_s technique", *J. Phys. G* **28** (2002) 2693, doi:10.1088/0954-3899/28/10/313.